
Experimental Study on Seawater Freeze Desalination Based on Ultrasonic Vibration

Han Yuan[a,*], Suyun Yi[a], Qizhi Gao[a] and Haibin Wang[b]

a Marine Engineering, College of Engineering, Ocean University of China, 238 Songling Road, Laoshan district, Qingdao, 266100, China

b Naval Architecture and Marine Engineering, University of Strathclyde, Glasgow G4 0LZ, United Kingdom

* Corresponding author

Phone/Fax: +86-532-66781105,

E-mail: hanyuan@ouc.edu.cn (Han Yuan)

Address: 238 Songling Road, Laoshan district, Qingdao 266100, China

Abstract

Seawater freeze desalination is a promising technology with low energy consumption; however, the presence of salt inclusions during the freezing process presents a challenge to enhancing desalination efficiency. While ultrasonic vibration has been proven effective in reducing the supercooling degree and energy consumption in pure water freezing, its impact on seawater desalination efficiency remains to be investigated. This study experimentally explores the characteristics of seawater freeze desalination under ultrasonic vibration. An ultrasonic-assisted seawater freeze crystallizer was designed, and experiments were conducted to compare and analyze the freeze desalination performance of the crystallizer with and without ultrasonic vibration. The findings reveal that ultrasonic vibration significantly enhances desalination by promoting the formation of smaller ice crystals, resulting in a substantial increase in desalination rates ranging from 18.18% to 67.86%, with an average improvement of approximately 32.62%. Additionally, the application of ultrasonic vibration accelerates the icing process by approximately 8%. Notably, during continuous desalination operations, the effectiveness of ultrasonic vibration gradually diminishes as salinity decreases. Nonetheless, the ultrasonic vibration-based freeze-reverse osmosis (Ultrasonic-Freeze-RO) method offers significant advantages in terms of reduced costs and energy consumption compared to both freeze-reverse osmosis (Freeze-RO) and traditional reverse osmosis (RO) methods.

Keywords: ultrasonic vibration; freeze desalination; experimental study; energy consumption

1 Introduction

According to statistics, seawater accounts for 97.5% of the total water on Earth, and this saline water is difficult to be directly used for irrigation, drinking, and industrial purposes. The remaining 2.5% of freshwater, of which only less than 1% is available for use[1, 2]. With the continuous growth of the world's population and industrial development, the global demand for freshwater is increasing, leading to a global freshwater shortage. The Millennium Development Goals Report pointed out that in 2015, approximately 40% of the global population faced water scarcity, and this number is expected to continue to rise[3]. Therefore, utilizing and developing the abundant seawater resources into freshwater can significantly alleviate the freshwater crisis, leading to the emergence of seawater desalination technology[4, 5]. Currently, the commonly used methods for seawater desalination are reverse osmosis (RO) and thermal methods, particularly multi-stage flash distillation (MSF) and multi-effect distillation (MED) are widely applied in large-scale seawater desalination plants[6, 7]. However, these seawater desalination technologies mentioned above are prone to severe scaling issues and have relatively high energy requirements[8, 9].

In recent years, the freezing desalination technology has been considered as one of the most promising seawater desalination technologies. The freezing desalination technology utilizes the theory of solid-liquid equilibrium to desalinate saline seawater.

Its advantages lie in low energy consumption and environmental, with energy consumption only about one-seventh of that of thermal desalination [10]. Generally, in the presence of inorganic salt components in a water solution, the crystallization temperature is lowered. As the temperature decreases, the water in the solution will first freeze, obtaining pure water without impurities as a solid phase separation. The inorganic salts and other impurities will continue to remain in the solution, and through solid-liquid separation, ice with lower salinity and concentrated brine with higher salinity can be obtained, achieving the purpose of desalination[11]. Figure 1 shows a schematic diagram of a binary water-salt system. Point D represents the eutectic point, where ice, salt, and saturated solution coexist. When a solution with solute mass concentration W_A at temperature T_A decreases to T_B (liquid phase line), ice phase begins to precipitate. As the temperature continues to decrease, the solution gradually enriches along line BC to the eutectic point D, during which the amount of ice increases continuously, and the remaining saline water's salinity increases. Upon reaching point D, salt crystals and ice crystals precipitate simultaneously. Below the eutectic point, salt hydrates and ice are generated simultaneously without leaving any liquid[12].

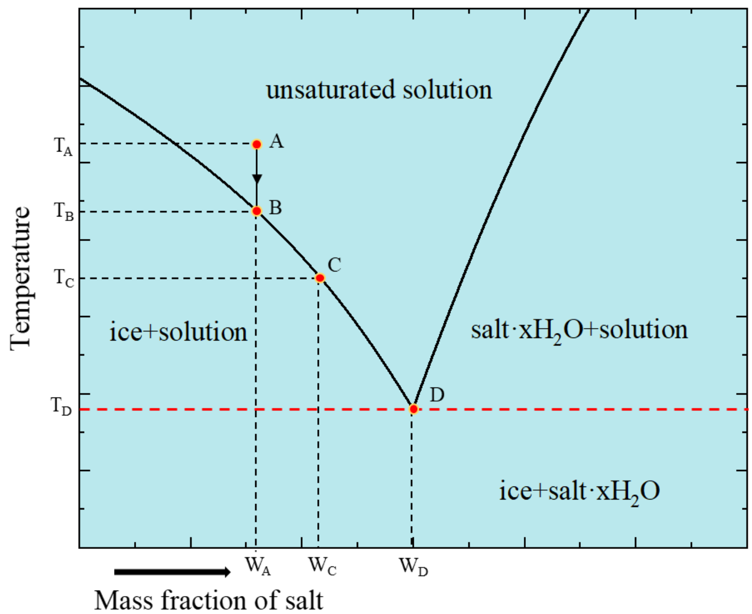

Figure 1 Binary water-salt system phase diagram

In addition, the ice crystals generated in the process of freezing desalination can also be used to store cold energy to meet the needs of refrigeration and food refrigeration[13]. Some scholars have studied the application of freezing desalination in the treatment of desulfurization wastewater[11], concentrated apple juice[14], wine production[15] and cold energy utilization of LNG[16].

Common methods for seawater freezing desalination typically include direct contact and indirect contact methods. The direct contact method involves direct contact between the refrigerant and seawater, causing freezing on the contact surface and producing ice crystals, thereby obtaining solid freshwater with lower salinity. For example, using silicone oil, natural gas, etc., as refrigerants to obtain ice with lower salinity[17, 18]. The advantages of the direct contact method are high ice production rate and low power consumption. However, its disadvantages are also significant, as it requires additional separation methods to separate ice crystals and refrigerants, such as washing. This undoubtedly leads to certain losses. The indirect contact method uses a heat-conducting solid surface to separate the refrigerant from the saline water, eliminating the need for additional washing or treatment processes.

Many scholars have conducted relevant research on indirect contact seawater freezing desalination[7]. Eghtesad[19] conducted numerical studies and multi-objective optimization on indirect freezing seawater desalination, suggesting that the refrigeration capacity has a certain impact on the recovery rate and desalination rate. A larger refrigeration capacity leads to an increase in ice crystal production and recovery rate, but more salt crystals are trapped in the gaps of the ice crystals, resulting in a decrease in desalination rate. In other words, the desalination rate and recovery rate constrain each other. Jayakody[20] modeled and simulated indirect seawater freezing desalination using an ice maker to study the effects of freezing temperature and initial salinity of the saline water on ice crystal production and the final salinity of ice and brine. As the freezing temperature decreases, the low temperature increases ice production, accelerates the freezing rate of saline water, and enhances the solidification rate. It is believed that using two-stage freezing desalination can effectively obtain low salinity freshwater. Yuan and Sun[21] conducted experimental research on a ship exhaust waste heat-driven seawater freezing desalination system as a pre-desalination for reverse osmosis desalination, and found that a two-stage freezing desalination system as a pre-desalination for reverse osmosis desalination has good economic benefits. In addition, some scholars have used various technological improvements to increase the desalination rate of the produced ice crystals, such as centrifugal separation[22], washing[23], sweating[24], and comprehensive methods[25]. These technologies can significantly improve the desalination rate of seawater but lead to a significant decrease in seawater recovery rate.

In current research, although low-temperature seawater freezing desalination technology offers advantages such as ease of operation and environmental friendliness, its desalination efficiency is relatively low, necessitating the use of additional methods for auxiliary treatment. Some scholars have explored the use of nucleating agents to accelerate the formation of ice crystals, thereby reducing the amount of salt trapped in the ice crystals and improving the desalination effectiveness[26, 27]. However, this approach can increase the operational costs of the freezing desalination system and require additional steps for removing the nucleating agents, thereby increasing the complexity of wastewater treatment.

Ultrasound is a high-frequency sound wave characterized by strong penetrative properties. When positive and negative pressure waves generated by ultrasound propagate in a liquid and reach a certain intensity, they create cavitation bubbles (negative pressure) and bubble collapse (positive pressure) within the liquid. After multiple cycles, the tiny cavitation nuclei inside the liquid undergo a series of oscillation, growth, collapse, and fragmentation processes. Studies have shown that the cavitation effect generated by ultrasound vibration can influence the degree of solution undercooling and saturation, effectively enhancing the cold energy diffusion in the system and providing nucleation sites, thereby improving the effectiveness of freezing desalination[28-31].

However, a notable research gap exists in the scarcity of studies exploring the effect of ultrasonic vibration on desalination during seawater freezing, considering the intricate mass transfer and desalination dynamics inherent in this process. To date, among the few studies conducted, Phelan [32] focused exclusively on the ultrasonic freezing behavior of pure water, demonstrating that ultrasonic waves significantly decrease the supercooling required for water to freeze and shorten the freezing duration, thus reducing overall freezing energy consumption. Specifically, the application of 197 J and 462 J of ultrasonic energy resulted in energy savings of 12.4% and 10.8%, respectively. This characteristic establishes a robust foundation for the potential utilization of ultrasonics in seawater desalination through freezing methods. Furthermore, Zhang [33] conducted experimental research on the desalination behavior of sea ice melting enhanced by ultrasonic vibration, verifying that it accelerates the melting speed and improves the removal efficiency of total dissolved solids (TDS) and salt from sea ice, suggesting further opportunities for exploiting ultrasonic vibration during sea ice melting processes. Nevertheless, despite these initial insights, no research has yet specifically addressed the influence of ultrasonic vibration on the desalination efficacy during the actual freezing process of seawater.

In this manuscript, to further investigate the relationship between ultrasound vibration and its impact on desalination rate and ice formation rate in the seawater freezing desalination process, we selected three independent variables: freezing temperature, freezing time, and seawater salinity. We constructed an experimental platform for ultrasound-assisted seawater freezing desalination and designed and conducted orthogonal experiments. To control the temperature of the freezing medium, a compression refrigeration unit was used to control the temperature of the glycerol-water solution in the storage tank. The main objective of this work is to verify the promoting effect of ultrasound vibration on the desalination efficiency of seawater inside the tube, establish relevant fitting equations, and study the economic feasibility of ultrasound-assisted secondary seawater desalination as a pre-desalination method for reverse osmosis desalination.

In the part 2 of this manuscript, detailed information about the experimental setup is provided. The part 3 introduces the experimental principles and analysis processes. The part 4 presents the experimental results and conducts data analysis.

2 Experimental setups

The schematic diagram of the ultrasonic freezing desalination system is shown in Figure 2. The experimental setup consists of two main sections: the refrigeration cycle system and the seawater freezing desalination experimental system. In the refrigeration cycle system, a compressed refrigeration cycle is employed to cool a glycerol-water mixture in the cold storage tank, which acts as the cold source medium for seawater freezing. The heat transfer medium in the cold storage tank is a 66.7% glycerol-water solution, which is pumped into the freezing crystallizer device through a cooling medium pump to freeze the seawater. The ultrasonic generator is used to adjust the frequency and power output of the ultrasonic oscillator. The data acquisition module monitors experimental data in real time. The controller is used to coordinate the operation of various components and record data. Further detailed information on the components of the test stand will be provided in the subsequent sections.

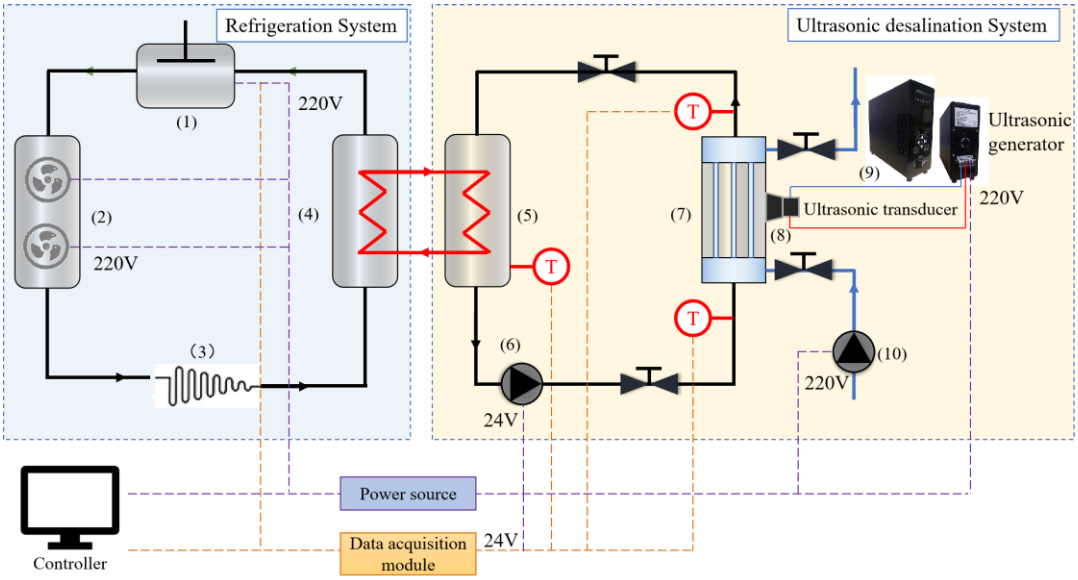

Figure 2 Schematic diagram of the ultrasonic freezing desalination system: (1) compressor, (2) condenser, (3) capillaries, (4) evaporator, (5) cold storage tank, (6) glycerin solution pump, (7) freezing crystallizer, (8) ultrasonic transducer, (9) ultrasonic generator, (10) seawater pump; (b) experimental setup

2.1 Seawater freezing desalination experimental system

The experimental setup of the ultrasonic freezing desalination system is shown in Figure 3. To minimize the impact of external environmental temperature on the working fluid inside the pipes and heat exchangers, adequate insulation measures were implemented using foam boards and thermal insulation materials. Additionally, low-temperature phase change materials (PCM) were placed to further reduce the internal temperature of the experimental setup. All cooling medium pipelines in the experimental setup are made of 3-inch PE pipes with corresponding quick couplings, ensuring good sealing and insulation. The connection between the cooling medium pipelines and the heat exchangers is achieved using stainless steel 304 tower heads and rubber hoses. The seawater channel employs a backflow structure, regulating the flow of seawater into the freezing desalination experimental device by adjusting the valve opening at the inlet of the heat exchanger.

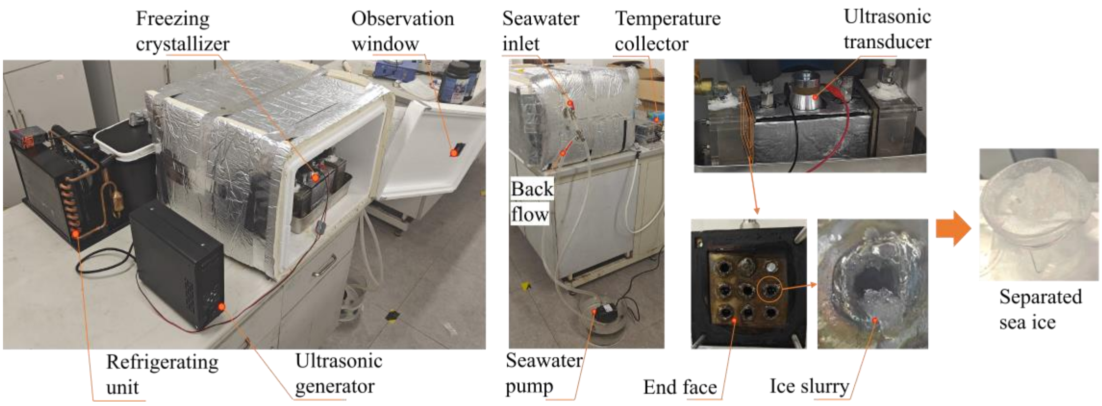

Figure 3 Experimental setup of the ultrasonic freezing desalination system

The cooling medium pump in this experimental setup is a small gear oil pump with a pure copper pump head. This gear pump operates at a rated voltage of 24V and a rated current of 3.2A, controlled by an adjustable voltage and current DC power supply, and it transports the cooling medium (glycerol-water solution) to the freezing crystallizer.

The temperature acquisition module uses the Sulinkiot 8-channel thermocouple data acquisition module, which reads the potential difference signals generated by the thermocouple due to the thermoelectric effect and converts them into temperature signals. These temperature data can be transmitted to the computer system via a USB to RS486 module. A T-type ultra-fine thermocouple is used to collect the temperatures at the inlet and outlet of the heat exchanger, monitoring the temperature of the glycerol at the inlet and outlet of the freezing crystallizer. This setup aims to obtain the temperature curve of the heat exchanger when it reaches a steady state. Programming is conducted in Python to collect, output, and save the temperature signals generated by the temperature acquisition module every 2 seconds.

The ultrasonic generator converts electrical energy into high-frequency alternating current signals that match the ultrasonic transducer, transmitting them to the ultrasonic oscillator, and converting the input electrical power into ultrasonic waves for transmission. The ultrasonic oscillator has a specific frequency, and the ultrasonic generator must generate electrical signals of the corresponding frequency to prevent reverse electromagnetic force, which could damage the ultrasonic generator. In this experimental setup, the KMD-M3 ultrasonic generator is selected, with an adjustable frequency range of 17-120 kHz. According to reference [34], the application of high-frequency ultrasound results in an increase in heat generated by the ultrasonic thermal effect. Additionally, the rise in ultrasonic frequency during the freezing process extends the growth cycle of cavitation bubbles, introducing new physical phenomena that are detrimental to the study of desalination characteristics. Therefore, a 40 kHz ultrasonic transducer with a power of 60W was selected for the experiment.

The list of the main experimental equipment and data acquisition devices used in this study is shown in Table 1.

Table 1 List of experimental equipment and measurement device parameters

Name	**Manufacturer**	**Model**	**Parameters**
T-type Micro Thermocouple	Aidewin	T-type 1m Welding Pin	-200~200℃, ±0.1℃
Temperature Data Acquisition Module	Sulingke	RS20K-C	±1℃
USB to RS485 Converter	Sulingke	—	CH340 Chip
Gear Pump	Guojiang New	FP-24	24V 3.2A

Name	**Manufacturer**	**Model**	**Parameters**
	Energy		
Ultrasonic Generator	KMD	KMD-M3	17-120kHz
Ultrasonic Transducer	KMD	—	40kHz 60W
Seawater Submersible Pump	SoulLi	—	35W

2.2 Ultrasonic freezing crystallizer

The schematic diagram and setup picture of the ultrasonic freezing crystallizer for seawater desalination is shown in Figure 4, which features a shell-and-tube heat exchanger structure. To ensure relatively high and consistent heat transfer efficiency, a counter-current heat exchange method is uniformly adopted in this experiment. The materials for the inner tube, baffle plate, and outer wall of the heat exchanger are all stainless steel 304. The inner tube has an inner diameter of 9 mm, a length of 16 cm, and a wall thickness of 1 mm, while the baffle plate and outer wall have a thickness of 3 mm. These components are fixed and connected using argon arc welding. The outer surface of the heat exchanger is insulated with a 1 cm thick layer of thermal insulation cotton.

The seawater inlet and outlet are located on both sides of the device and are made of acrylic material. These parts are fixed and sealed to the heat exchanger using screws and rubber pads to prevent seawater leakage. The ultrasonic oscillator is installed at the center of the upper wall surface, as shown in the diagram, and is fixed and connected using a special adhesive designed for ultrasonic oscillators.

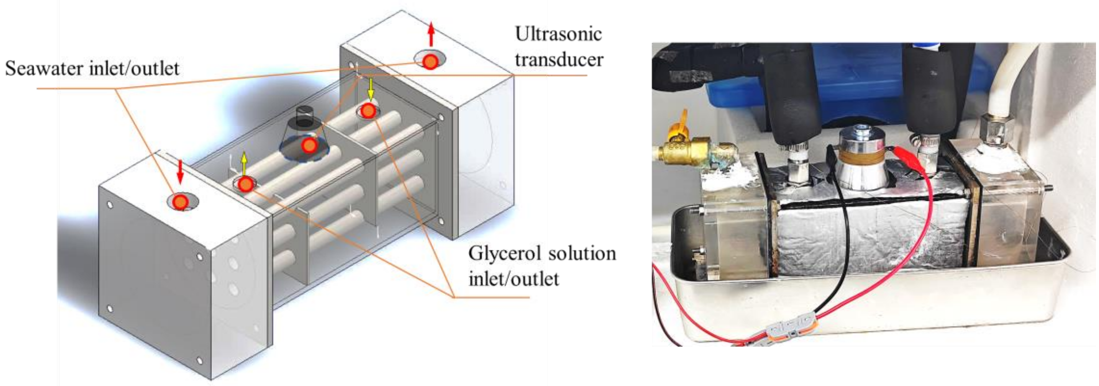

Figure 4 Schematic and setup picture of the ultrasonic freezing crystallizer for

seawater desalination

2.3 Refrigeration cycle system

The refrigeration cycle system in the experiment consists of a compressor, condenser, evaporator, cold storage tank, temperature control module, and associated pipelines. Its primary function is to lower the temperature of the glycerol-water solution in the cold storage tank, maintain the temperature and stability of the cooling medium, and serve as the freezing medium in the seawater crystallizer. The structure of the refrigeration unit is depicted in Figure 5. The cooling power of the refrigeration unit is 165W, utilizing R134a as the refrigerant, with a minimum cooling temperature of -40°C.

The condenser is an air-cooled condenser, powered by a 220V AC motor with a 40W rating. The evaporator consists of a copper coil placed directly inside the reservoir, allowing for the direct cooling of the glycerol-water solution as the cooling medium. The reservoir has dimensions of 420 mm × 370 mm × 240 mm. The refrigeration unit is equipped with a temperature control module that monitors the temperature using a probe inside the liquid reservoir. This module regulates the temperature within the reservoir by controlling the compressor power switch. The temperature control module selected for this test bench has a control range of -50°C to 110°C (±0.1°C), with a temperature control differential set at 0.5°C.

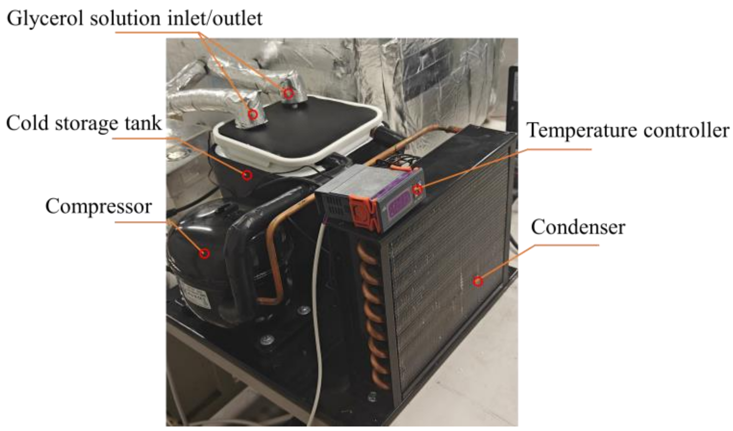

Figure 5 Refrigeration cycle system composition view

The main component of glycerol is propane-1,2,3-triol, which is easily soluble in water. Its aqueous solution has a lower freezing point, making it an excellent antifreeze and refrigerant. The freezing point of glycerol-water solution can be calculated as follow:

$$\Delta T_f = T_f^* - T_f = K_f \cdot m \quad (1)$$

where K_f represents the cryoscopic constant (freezing point depression constant); m denotes the molal concentration.

Table 2 provides the freezing points of glycerol-water solutions at different mass concentrations. It can be observed that the freezing point of glycerol-water solutions shows an initial increase followed by a decrease as the concentration of glycerol increases. In this study, a glycerol-water solution with a concentration of 66.7% was selected, which exhibited the lowest freezing point of -46.5°C.

Table 2 Freezing point of glycerol-water solution

Glycerol mass fraction (%)	10	30	50	66.7	80	90
Freezing point (°C)	−1.6	−9.5	−23.0	−46.5	−20.3	−1.6

3 Experimental design and evaluation methods

The seawater used in the experiment was prepared by dissolving different amounts of seawater blending salt into distilled water. Table 3 shows the ion composition and physical properties of the seawater when 1 kg of seawater blending salt is dissolved in 30 kg of distilled water. The mass of the salt was measured using a digital balance with a capacity of 300 g and an accuracy of 0.01 g. The salinity of the seawater was measured using a SMART SENSOR AR8012 salinity meter, which has a range of 0-100 ppt (parts per thousand) and an accuracy of ±3% F.S ±1 digit. The seawater temperature and flow rate were maintained at constant levels, with the inlet seawater temperature kept around room temperature (20°C) and the initial seawater flow rate controlled at 1 ml/s.

Table 3 Physical data and ionic composition of artificial seawater

Component	**Values**	**Units**	**Component**	**Values**	**Units**
Specific gravity	1.020-1.022(25°C)	-	Na^+	9100-9300	mg/L
Salinity	30-31(25°C)	ppt	Mg^{2+}	1150-1250	mg/L

PH	8.20-8.50(25℃)	-	Ca^{2+}	380-420	mg/L
Total alkalinity	2.9-3.5	mmol/L	K^{+}	240-355	mg/L
KH	8.0-10.0	dKH	Sr^{2+}	8.2-9.0	mg/L
Cl^{-}	17150-17980	mg/L	Br^{-}	40-55	mg/L
SO_4^{2-}	2250-2350	mg/L	F^{-}	0.9-1.1	mg/L
HSO_4^{-}	120-135	mg/L	B^{3+}, B^{5+}	5.0-6.0	mg/L

The comparative experimental study of freezing desalination with and without ultrasonic vibration was designed. In order to optimize the relationship between various factors during the experimental process, to systematically arrange the experimental procedure, analyze experimental data, and achieve optimal experimental results with a minimized number of trials, an orthogonal experimental design [35] was implemented. This method aims to uncover the internal relationships among experimental variables while efficiently reducing the number of experiments required.

3.1 Orthogonal experimental design

In this study, careful consideration was given to the impact of three key factors: the temperature of the glycerol-water solution in the cold storage tank, the salinity of seawater at the inlet of the crystallizer, and the freezing time, on the process of seawater freezing desalination. Each factor was examined at five different levels, employing an $L_{25}(5^6)$ orthogonal experimental design table. The specific values for each level of the experimental factors are detailed in Table 4.

Table 4 Each level of experimental factors

Experimental factor level	L1	L2	L3	L4	L5
Inlet salinity x/ppt (parts per thousand)	15	20	25	30	35
Freezing temperature T/°C	−9	−12	−15	−18	−21
Freezing time t/s	100	125	150	175	200

The design of the orthogonal table is presented in Appendix, where factors A to C in Appendix represent the salinity of the inlet seawater in the cold storage tank, the temperature of the propylene glycerol-water solution, and the freezing time, respectively. Experiments were conducted separately without using ultrasonic vibration and with ultrasonic vibration. The experimental results were output as the desalination rate of the freezing seawater and the ice production rate inside the heat exchanger. Range analysis and variance analysis were performed on the experimental data, and the experimental data processing and analysis were validated using SPSS orthogonal analysis software.

3.2 Evaluation methods

The desalination rate of the freezing seawater is defined as the difference in salinity between the seawater at the inlet and the seawater after the crystalline product has melted following freezing desalination. The salinity of the inlet sea water is x, and the salinity of the frozen sea water in the pipe after melting is x'. The desalination rate of the freezing seawater is given by:

$$w = \frac{x - x'}{x} \times 100\% \quad (2)$$

The seawater icing rate is defined as the ratio of the volume of the crystalline product after freezing desalination to the total volume inside the pipe. The volume of seawater in the tube after melting is V_{ice}, and the total volume in the heat exchanger tube is V, then the icing rate inside the heat exchanger is:

$$y = \frac{V_{ice}}{V} \times 100\% \quad (3)$$

Range analysis is a commonly used method for handling orthogonal experimental results, which can intuitively demonstrate the extent to which different factors affect the experimental results. The principle involves analyzing the total response value K and the average response value k of each factor at different levels of influence. The total response value K represents the sum of the experimental values of a factor at the i-th level, while the average response value k is the average value of K corresponding to the level number i. It is generally believed that a larger average response value k indicates a better effect of the corresponding factor at that level. The range *R* value is the difference between the maximum and minimum values of the average response value *k*, and a larger *R* value indicates a greater impact of that factor on the experimental results.

Range analysis can intuitively reveal the differences in experimental results corresponding to different levels of various factors. However, this analysis process cannot distinguish whether these differences are due to variations in the levels of the factors or due to errors. To analyze the magnitude of errors that inevitably exist in the experimental process, variance analysis is often employed. Variance analysis calculates the sum of squares of deviations S_j for each factor and error and the degrees of freedom *f*, thereby obtaining the mean square $\hat{S}_j$ and *F* values for each factor and error. By consulting the *F*-test critical value table, the F_α values for each factor are determined, ultimately establishing the significant level of the corresponding factor. These evaluation parameters are shown in Equation (4) to (8):

$$S_j = \frac{\sum_{i=1}^{m} K_i^2}{m} - \frac{\left(\sum_{i=1}^{n} z_i\right)^2}{n} \tag{4}$$

$$f_{total} = nm - 1 \tag{5}$$

$$f_j = m - 1 \tag{6}$$

$$\hat{S}_j = \frac{S_j}{f_j} \tag{7}$$

$$F = \frac{\hat{S}_j}{\hat{S}_{error}} \tag{8}$$

where *m* is the selected factor corresponds to the number of levels, *n* is the number of experiments, z_i is the result of the *i*-th experiment.

3.3 Uncertainty analysis

The error transfer principle is used to analyze the uncertainty of the experimental results:

$$\frac{\Delta_w}{w}=\sqrt{\left(\frac{\partial \ln w}{\partial x}\right)^2\left(\Delta_x\right)^2\cdot+\left(\frac{\partial \ln w}{\partial x'}\right)^2\left(\Delta_{x'}\right)^2} \tag{9}$$

$$\frac{\Delta_y}{y}=\sqrt{\left(\frac{\partial \ln y}{\partial V}\right)^2\left(\Delta_V\right)^2\cdot+\left(\frac{\partial \ln y}{\partial V_{ice}}\right)^2\left(\Delta_{V_{ice}}\right)^2} \tag{10}$$

Based on the accuracy of the measuring devices, the uncertainty of all experimental data obtained is less than 3.99%, ensuring high reliability.

4 Results and discussion

The characteristics of seawater freeze desalination with and without the application of ultrasound were experimentally compared and investigated in this study. Identical equipment was used in the control experiments to ensure the comparability of the results.

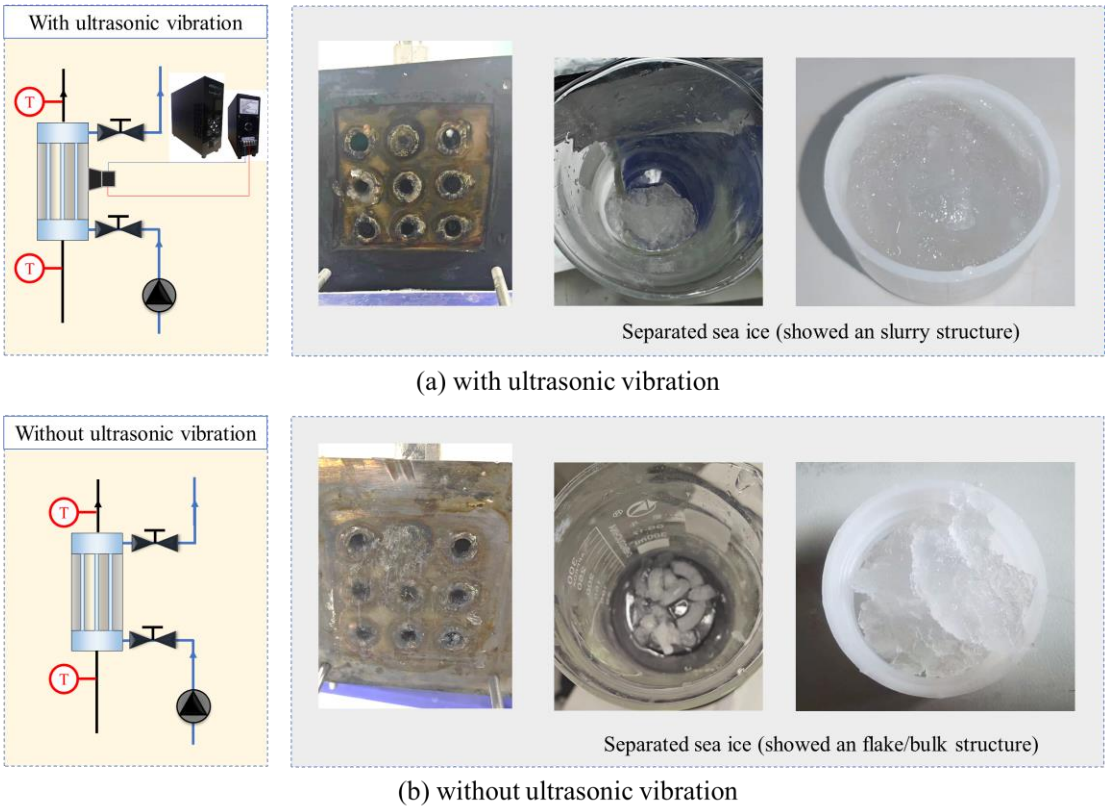

Figure 6 Sea ice with and without ultrasonic vibration

Figure 6 shows the sea ice morphology obtained from the experiment. Overall, the use of ultrasonic vibration can effectively fluidized sea ice without causing blockages in heat exchanger tubes. When ultrasonic vibration is not applied, the freezing of seawater will present a sheet-like or block like structure, which is prone to tube blockage.

4.1 Seawater freezing desalination without ultrasonic vibration

Table 5 to Table 8 show the experimental results and range analysis of seawater desalination by freezing without ultrasonic vibration.

Table 5 Results of orthogonal experiment without ultrasonic vibration

Group	$w/\%$	$y/\%$	Group	$w/\%$	$y/\%$	Group	$w/\%$	$y/\%$
1	26.14	40.15	**10**	19.50	65.45	**19**	15.15	64.09
2	30.32	63.79	**11**	20.24	50.15	**20**	12.08	72.27
3	24.83	70.91	**12**	21.12	76.52	**21**	15.34	62.42
4	19.08	80.91	**13**	15.20	80.61	**22**	20.45	45.75
5	13.16	85.91	**14**	18.73	58.94	**23**	20.51	60.15
6	27.00	48.18	**15**	18.97	70.30	**24**	15.43	70.61
7	23.47	65.45	**16**	16.56	58.18	**25**	10.42	78.94
8	18.69	72.73	**17**	20.34	72.12			
9	14.50	84.85	**18**	18.67	56.67			

According to the range analysis in Table 6, the three influencing factors—salinity of the inlet seawater, temperature of the glycerol-water solution in the storage tank, and freezing time—affect both the seawater desalination rate and the icing rate of the heat exchanger tubes to varying degrees. For the seawater desalination rate, the order of influence from greatest to least is T > t > x, with the maximum range being 8.31 and the minimum range being 6.28, indicating a similar level of influence among the factors. Regarding the icing rate of the heat exchanger tubes, the order of influence is t > T > x, with freezing time and temperature having a significantly greater impact than seawater salinity.

Table 6 Range analysis results without ultrasonic vibration

Experimental parameter	Inlet salinity/ppt		Freezing temperature/°C		Freezing time/s	
	$w/\%$	$y/\%$	$w/\%$	$y/\%$	$w/\%$	$y/\%$
K_1	113.54	341.67	105.28	259.09	103.49	266.97
K_2	103.16	336.67	115.70	323.64	111.96	306.52
K_3	94.25	336.52	97.90	341.06	96.05	329.39
K_4	82.79	323.33	82.88	359.39	85.86	367.27
K_5	82.16	317.88	74.13	372.88	78.54	385.91
k_1	22.71	68.33	21.06	51.82	20.70	53.39
k_2	20.63	67.33	23.14	64.73	22.39	61.30
k_3	18.85	67.30	19.58	68.21	19.21	65.88
k_4	16.56	64.67	16.58	71.88	17.17	73.45
k_5	16.43	63.58	14.83	74.58	15.71	77.18
R	6.28	4.76	8.31	22.76	6.68	23.79

To visually analyze the relationship between these influences and the experimental results, the factor levels are plotted on the horizontal axis, and the average response values corresponding to the seawater desalination rate and tube icing rate are plotted on the vertical axis. The results are shown in Figure 7.

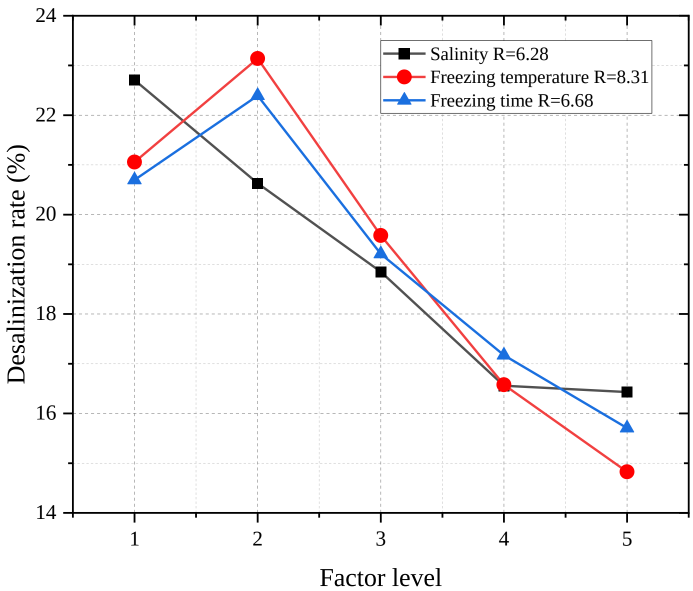

(a)

This is the author accepted manuscript of: Yi, S., Gao, Q., Song, J., Wang, H., & Yuan, H. (2025). Experimental study on seawater freeze desalination based on ultrasonic vibration. *Desalination*, *596*, Article 118336. https://doi.org/10.1016/j.desal.2024.118336. For the purposes of open access, a CC BY 4.0 licence has been applied to the manuscript.

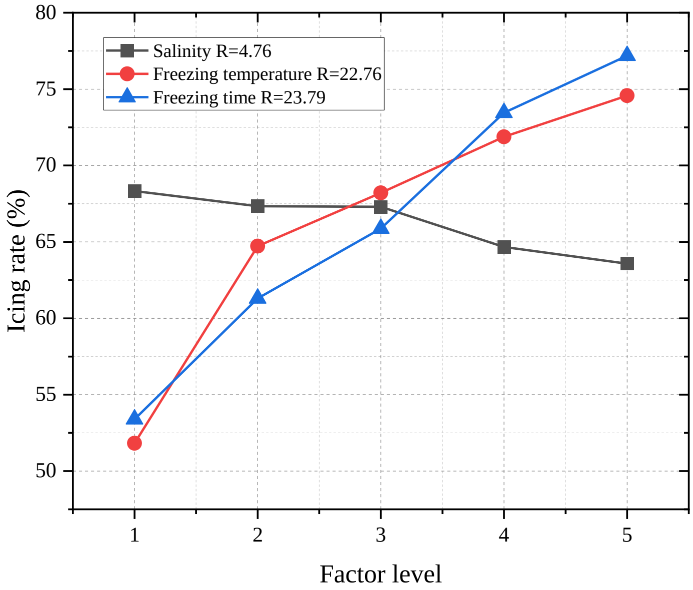

(b)

Figure 7 The average response values of each factor level in the experiment without ultrasonic vibration (a) desalting rate (b) icing rate

As illustrated in Figure 7(a), the relationship between each factor and the desalination rate is detailed. Inlet seawater salinity shows the least impact on the seawater desalination rate, with an R-value of 6.28. As inlet seawater salinity increases, there is a gradual decrease in the seawater desalination rate.

The freezing time during the heat exchange process exhibits a slightly higher influence on the seawater desalination rate compared to inlet seawater salinity, with an R-value of 6.68. Initially, the desalination rate increases with longer freezing times, peaking at 125 seconds. However, at shorter freezing times, seawater tends to crystallize, resulting in a lower desalination rate due to higher seawater content remaining with the sea ice during ice-water separation. As freezing time increases, more sea ice forms, including some concentrated seawater, which diminishes the desalination rate owing to increased concentration of seawater on the ice surface.

The temperature of the glycerol-water solution exerts the greatest impact on the seawater desalination rate, with an R-value of 8.31. Initially, the desalination rate rises with decreasing temperature, achieving optimal performance at a glycerol-water solution temperature of -12°C. However, excessively low temperatures lead to increased supercooling of seawater, causing rapid freezing during crystallization. This process results in salt pockets enclosed within ice crystals, ultimately reducing the desalination rate.

In Figure 7(b), the relationship between each factor and the heat exchanger tube icing rate is depicted. Freezing time has the most pronounced impact on the icing rate, with an R-value of 23.79. As freezing time increases, the icing rate inside the tube also rises. Similarly, freezing temperature significantly influences the icing rate, with an R-value of 22.76. Lower freezing temperatures correspond to higher icing rates. This is because longer freezing times and lower temperatures result in greater cooling of the seawater inside the tube, leading to increased icing.

Inlet seawater salinity also affects the tube icing rate, albeit to a lesser extent, with an R-value of 4.76. As seawater salinity increases, the tube icing rate decreases gradually. This relationship arises because higher seawater salinity lowers the freezing point of seawater, necessitating colder temperatures to initiate ice formation, thereby reducing the icing rate.

Table 7 Analysis of variance of desalting rate without ultrasonic experiment

Variance source	S_j	f_j	$\hat{S}_j$	F	F_α	Significant
Inlet salinity	144.87	4	36.22	12.67	2.88×10^{-4}	Significant
Freezing temperature	224.93	4	56.23	19.67	3.33×10^{-5}	Significant
Freezing time	143.04	4	35.76	12.51	3.06×10^{-4}	Significant
Error	34.30	12	2.86			

Note: $R^2 = 0.937$ (After the adjustment: $R^2 = 0.875$).

Based on the data from Tables 7 and 8, variance analysis reveals that the inlet seawater salinity, glycerol-water solution temperature, and freezing time significantly impact the seawater desalination rate. Furthermore, the glycerol-water solution temperature and freezing time also significantly affect the heat exchanger tube icing rate, whereas the inlet seawater salinity exerts a noticeable but lesser influence on the icing rate.

Table 8 Analysis of variance of icing rate without ultrasonic experiment

Variance source	S_j	f_j	$\hat{S}_j$	F	F_α	Significant
Inlet salinity	81.40	4	20.35	2.86	0.0706	non-significant
Freezing temperature	1577.24	4	394.31	55.45	1.22×10^{-7}	Significant
Freezing time	1806.49	4	451.62	63.51	5.66×10^{-8}	Significant
Error	85.33	12	7.11			

Note: $R^2 = 0.976$ (After the adjustment: $R^2 = 0.952$).

4.2 Seawater freezing desalination with ultrasonic vibration

Table 9 to Table 12 shows the experimental results and range analysis of seawater desalination by freezing after ultrasonic vibration.

Table 9 Results of orthogonal experiment with ultrasonic vibration

Group	$w/\%$	$y/\%$	**Group**	$w/\%$	$y/\%$	**Group**	$w/\%$	$y/\%$
1	36.36	55.33	**10**	24.38	75.50	**19**	22.15	75.33
2	40.52	77.17	**11**	29.60	68.67	**20**	20.13	86.83
3	32.67	80.33	**12**	25.30	86.83	**21**	27.67	81.67
4	19.87	93.00	**13**	16.80	95.50	**22**	29.91	59.67
5	13.16	97.67	**14**	25.00	69.17	**23**	27.51	70.17
6	31.84	61.33	**15**	25.79	80.00	**24**	22.57	88.00
7	27.27	80.83	**16**	27.76	73.67	**25**	12.25	94.50
8	25.62	88.83	**17**	24.25	88.67			
9	18.81	95.33	**18**	26.32	70.50			

According to the variance analysis presented in Table 10, the impact of ultrasonic vibration on the seawater desalination rate shows that the three factors are ranked in descending order of influence as T > t > x, with a range from 11.50 to 4.53. For the heat exchanger tube icing rate, the influence of the three factors is ranked in descending order as t > T > x. Specifically, freezing time and temperature significantly affect the icing rate more than seawater salinity, with ranges from 25.73 to 1.90.

Table 10 Range analysis results with ultrasonic vibration

Experimental parameter	Inlet salinity/ppt		Freezing temperature/℃		Freezing time/s	
	$w/\%$	$y/\%$	$w/\%$	$y/\%$	$w/\%$	$y/\%$
K_1	142.58	403.50	153.23	340.67	141.97	330.17
K_2	127.92	401.83	147.26	393.17	147.81	364.00
K_3	122.49	400.17	128.91	405.33	132.24	404.67
K_4	120.61	395.00	108.40	420.83	110.79	436.83
K_5	119.91	394.00	95.71	434.50	100.69	458.83
k_1	28.52	80.70	30.65	68.13	28.39	66.03
k_2	25.58	80.37	29.45	78.63	29.56	72.80
k_3	24.50	80.03	25.78	81.07	26.45	80.93
k_4	24.12	79.00	21.68	84.17	22.16	87.37
k_5	23.98	78.80	19.14	86.90	20.14	91.77
R	4.53	1.90	11.50	18.77	9.42	25.73

To visually analyze the relationship between these impacts and the experimental results, the average response values corresponding to the factor levels are plotted on the horizontal axis. The average response values for seawater desalination rate and tube icing rate are plotted on the vertical axis. These results are depicted in Figure 8.

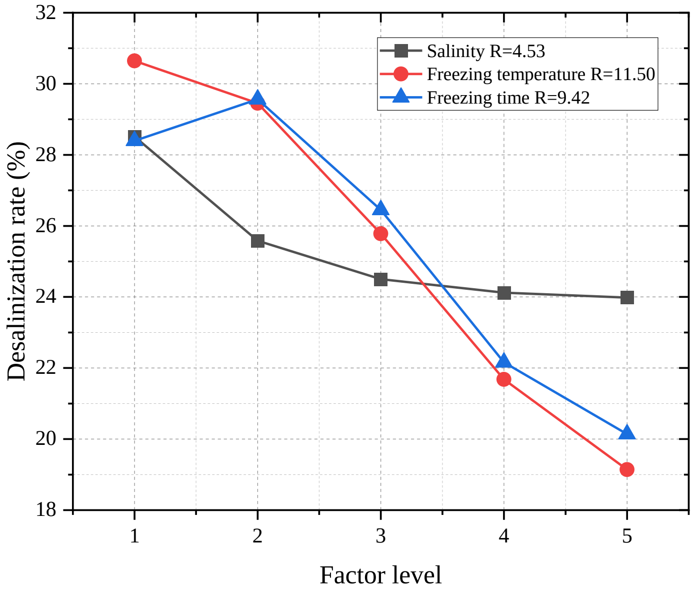

(a)

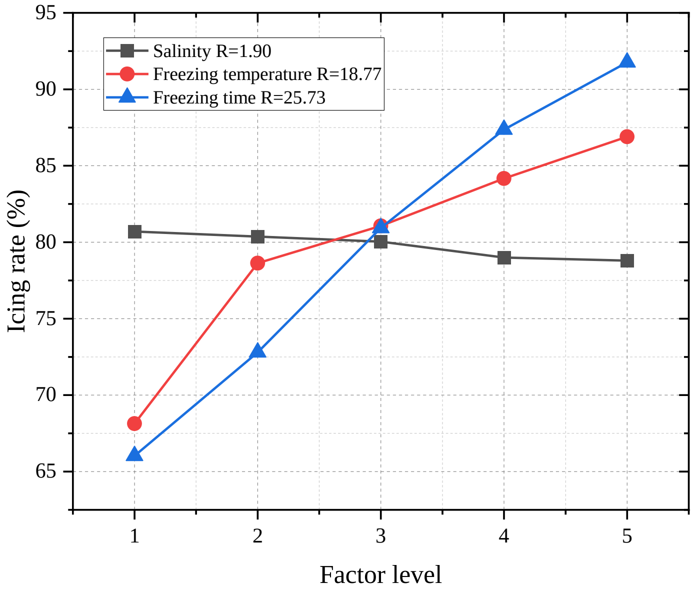

(b)

Figure 8 The average response values of each factor level in the experiment with ultrasonic vibration (a) desalting rate (b) icing rate

In Figure 8(a), the impact of inlet seawater salinity on the seawater desalination rate is minimal, indicated by an R-value of 4.53. The seawater desalination rate gradually decreases as inlet seawater salinity increases. Freezing time also affects the seawater desalination rate, with an R-value of 9.42. Initially, the desalination rate increases with freezing time, peaking at 125 seconds. The temperature of the glycerol-water solution exerts the greatest influence on the seawater desalination rate, with an R-value of 11.50. As freezing temperature decreases, the seawater desalination rate also decreases. Comparatively, the use of ultrasonic vibration enhances the desalination effect of seawater by generating finer ice crystals, thereby increasing the purity of frozen sea ice and reducing salt inclusion formation.

In Figure 8(b), the primary factors influencing the heat exchanger tube icing rate are freezing time and glycerol-water solution temperature, with R-values of 25.73 and 18.77, respectively. The influence of seawater salinity on the tube icing rate is minimal, with an R-value of 1.90. Ultrasonic vibration enhances ice crystal formation and facilitates the separation of water molecules and salt ions, significantly improving the tube icing rate compared to experiments without ultrasonic vibration.

Table 11 Analysis of variance of desalting rate with ultrasonic experiment

Variance source	S_j	f_j	$\hat{S}_j$	F	F_α	Significant
Inlet salinity	70.91	4	17.73	1.56	0.247	non-significant
Freezing temperature	485.34	4	121.34	10.68	6.32×10^{-4}	Significant
Freezing time	83.23	4	20.81	7.22	3.36×10^{-3}	Significant
Error	136.31	12	11.36			

Note: $R^2 = 0.866$ (After the adjustment: $R^2 = 0.733$).

Based on the data from Tables 11 and 12, variance analysis indicates that the temperature of the glycerol-water solution and freezing time significantly affect both the seawater desalination rate and the heat exchanger tube icing rate. In contrast, the impact of inlet seawater salinity on these rates is not statistically significant.

Table 12 Analysis of variance of icing rate with ultrasonic experiment

Variance source	S_j	f_j	$\hat{S}_j$	F	F_α	Significant
Inlet salinity	14.12	4	3.53	0.37	0.826	non-significant
Freezing temperature	1042.76	4	260.69	27.27	6.07×10^{-6}	Significant
Freezing time	2201.30	4	550.32	57.58	9.89×10^{-8}	Significant

Error	114.70	12	9.56

Note: $R^2 = 0.966$ (After the adjustment: $R^2 = 0.932$).

4.3 Performance comparison on freezing desalination with and without ultrasonic influence

Based on the aforementioned experimental data, it is clear that the optimal desalination effect occurs with a freezing time of 125 seconds. Furthermore, excessively low temperatures induce heightened supercooling of seawater, resulting in rapid crystallization and freezing. Therefore, experiments were specifically conducted with a freezing time of 125 seconds and a freezing temperature of -18°C for further analysis. The comparative experimental results are detailed in Table 13.

Table 13 Comparative experimental results between normal and ultrasonic based seawater freezing desalination

Salinity/ppt	$w/\%$		$y/\%$		Salinity/ppt	$w/\%$		$y/\%$	
	Normal	Ultrasonic	Normal	Ultrasonic		Normal	Ultrasonic	Normal	Ultrasonic
15	20.78	25.32	68.48	72.88	25	18.18	22.31	61.82	70.15
15	23.53	26.35	71.82	75.00	30	15.15	23.75	64.09	68.48
15	22.88	26.32	66.52	75.45	30	14.57	23.68	66.06	69.24
20	22.06	24.75	66.97	72.42	30	16.95	22.26	58.94	69.85
20	18.91	23.88	60.00	70.15	35	14.25	22.57	61.82	63.48
20	16.50	23.27	67.12	69.09	35	13.88	24.58	55.91	64.70
25	17.13	22.13	65.30	66.67	35	13.71	22.77	62.42	68.64
25	18.80	23.79	57.42	65.00					

Figure 9 shows the distribution of experimental points and the fitting curve. The range of R-squared values for the fitted equations is from 0.4518 to 0.8252. Among them, the fitting effect for seawater desalination rate is relatively good, while the fitting

This is the author accepted manuscript of: Yi, S., Gao, Q., Song, J., Wang, H., & Yuan, H. (2025). Experimental study on seawater freeze desalination based on ultrasonic vibration. *Desalination*, *596*, Article 118336. https://doi.org/10.1016/j.desal.2024.118336. For the purposes of open access, a CC BY 4.0 licence has been applied to the manuscript.

effect for the heat exchanger tube icing rate under ultrasonic experiments is moderate and acceptable within a certain range.

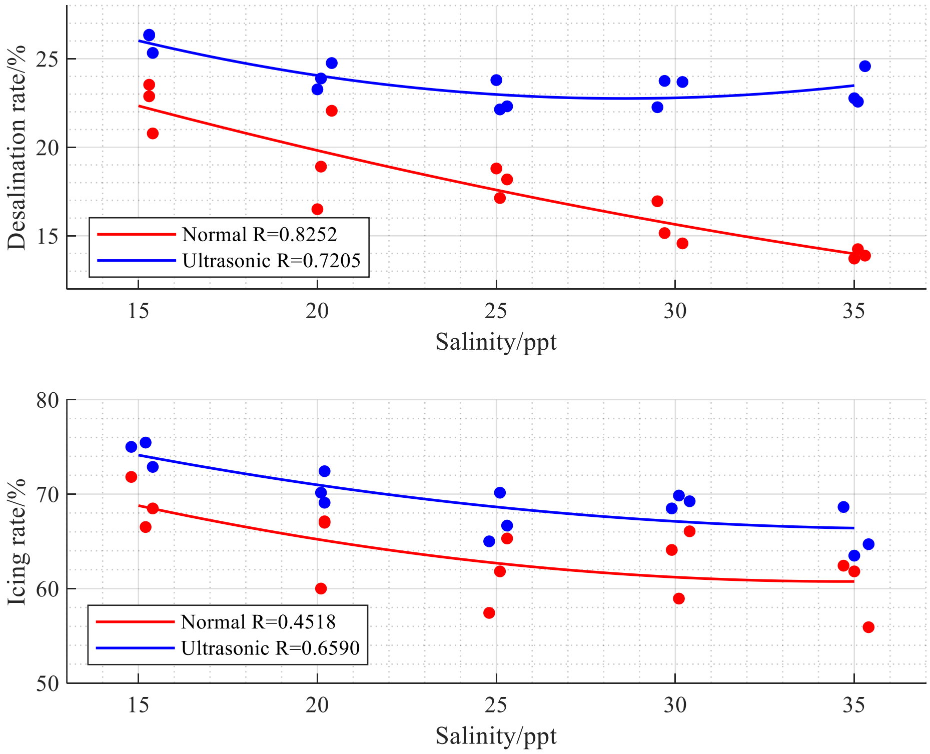

Figure 9 Fitting diagram of desalting rate and icing rate

Based on the above experimental results, the desalination rate and icing rate were fitted separately. The fitted equations for desalination rate and icing rate without the use of ultrasonic vibration are as follows:

$$w_0 = 0.005747x^2 - 0.705x + 31.62 \tag{11}$$

$$y_0 = 0.02075x^2 - 1.439x + 85.7 \tag{12}$$

With ultrasonic, the fitted equations for desalting rate and icing rate are as follows:

$$w_1 = 0.01771x^2 - 1.012x + 37.21 \tag{13}$$

$$y_1 = 0.01625x^2 - 1.199x + 88.46 \tag{14}$$

According to the competitive experimental results, ultrasonic freezing desalination substantially enhances desalination efficiency. Within the salinity range of 15-35 ppt, the desalination rate increased by 18.18% to 67.86%, with a more pronounced effect observed at higher salinity levels. The average desalination rate of ultrasonic one is 23.58%, compared with the normal one of 17.78%, and the average desalination rate increased by 32.62%. The icing rate also showed an increase of 8.03% to 8.20%. Moreover, the study also suggests that the enhancement effect of ultrasound on freezing desalination diminishes with increasing stages of desalination in continuous freezing desalination processes, especially after significant reduction in salinity. These results indicate promising prospects for the application of ultrasound technology in freezing desalination.

4.4 Economic analysis of ultrasonic based freezing desalination

The experimental research results above indicate that the use of ultrasonic freezing desalination technology can significantly enhance desalination efficiency. Since freezing desalination alone is insufficient to directly desalinate seawater to potable levels, it necessitates secondary desalination methods such as reverse osmosis (RO). In this condition, freezing desalination serves as a pretreatment process within a composite desalination system.

The thermodynamic and economic performance of a simple two-stage freeze desalination RO system is analyzed. After the seawater is pre-desalinated by two-stage ultrasonic freezing desalination equipment in turn, it flows into the RO system for final desalination. In order to simplify the calculation, other small component cost such as pumping and pipe are ignored, the system can be simply divided into freezing crystallization heat exchanger, ultrasonic machine and RO system. The power and cost of RO system can be calculated according to reference [36], shown in Table 14.

Table 14 Mathematical models of RO system.

Parameter	Equations
Recovery ratio	$RR = \frac{M_{fresh}}{M_{feed}}$
Rejected salt concentration	$X_{brine} = \frac{M_{feed} \times X_{feed} - M_{fresh} \times X_{feed} \times (1 - SR)}{M_{feed} - M_{fresh}}$

Temperature correction factor	$TCF = \exp\left(2700 \times \left(1/T - 1/298\right)\right)$
Membrane water permeability	$k_w = \dfrac{6.84 \times 10^{-8} \times (18.6865 - (0.177 \times X_{brine}))}{T}$
Osmotic pressure	$P_n = 75.85 \times X_n, n = feed, brine, fresh$
Net osmotic pressure across the membrane	$\Delta P_{os} = 0.5 \times (P_{feed} + P_{brine}) - P_{fresh}$
Net pressure difference across the membrane	$\Delta P_{net} = \left(\dfrac{M_{fresh}}{3600 \times TCF \times FF \times A_e \times n_e \times n_v \times k_w}\right) + \Delta P_{os}$
The required power input to the RO driving pump	$\dot{W}_{RO} = \dfrac{1000 \times M_{feed} \times \Delta P_{net}}{3600 \times \eta_p \times \rho_{feed}}$
Purchasing cost	$C_{RO} = C_k \times n_e \times n_v + C_{pv} \times n_v$

For heat exchanger, the cost calculation function is as follow[33]:

$$C_{hex} = 12000\left(\frac{A_{hex}}{100}\right)^{0.6} \tag{15}$$

where heat transfer surface area A_{hex} can be expressed as

$$A_{hex} = \frac{Q}{U \Delta T_{LMTD}} \tag{16}$$

$$\Delta T_{LMTD} = \frac{\Delta T_{\max} - \Delta T_{\min}}{\ln\left(\dfrac{\Delta T_{\max}}{\Delta T_{\min}}\right)} \tag{17}$$

where U is heat transfer coefficient, ΔT_{LMTD} is the logarithmic mean temperature difference, Q is heat flux, $\Delta T_{\max}$ and $\Delta T_{\min}$ are as follows:

$$\begin{cases} \Delta T_{\max} = \max\left(t_{hot,in} - t_{cold,out},\ t_{hot,out} - t_{cold,in}\right) \\ \Delta T_{\min} = \min\left(t_{hot,in} - t_{cold,out},\ t_{hot,out} - t_{cold,in}\right) \end{cases} \tag{18}$$

In addition, the energy consumption of ultrasonic machines is calculated as 1.8kWh based on large ultrasonic machines, and its maximum loading was 1000 kg[33]. The cost consumption of ultrasound is RMB5500 (765.53$), which is determined based on the large ultrasonic machine in actual production as an example.

In order to evaluate the performance of the system, the specific work consumption (SWC) and levelized cost of water (LCOW) of the system are expressed as,

$$SWC = \frac{W_{Ultrasound} + W_{RO}}{m_{fresh}} \tag{19}$$

$$LCOW = \frac{CRF \cdot C_{investment} + OMC}{t_{if} \cdot m_{fresh}} \tag{20}$$

Where capital recovery factor (CRF) is expressed as,

$$CRF = \frac{i(1+i)^n}{(1+i)^n - 1} \tag{21}$$

The Annual operation and maintenance costs (OMC) generally takes 6% of total cost. i is the annual loan interest rate, which is set as 8%, n denotes the life cycle time, which is set as 20 years in this study, t_{if} is the load factor, considering the influence of disastrous weather in coastal areas, the value of 7000 hours is taken[37].

With the daily output fresh water of 1000m^3/day as the desalination target. The South Pacific region is selected for research. The average salinity of seawater is 35 ppt. Desalination results of ultrasonic/no ultrasonic freezing desalination are calculated according to formula (11)-(14). The basic operating conditions of the design system are given according to reference [33], shown in the Table 15.

Table 15 Operating parameters of the proposed CCDP system

Parameter	Value
heat transfer coefficient/ kW·m^{-2}·K^{-1}	1.1
Inlet Seawater salinity/ ppt	35
Recovery ratio/ %	30
Effective area of membrane/m^2	37
Number of membrane elements	7
Number of pressure vessel	9
Price of each membrane/ $	1200
Price of pressure vessel/ $	7000

High pressure pump efficiency	90
Fouling factor	80
Price of ultrasound/ $	765.525

Table 16 shows the performance of various desalination systems. Compared with ordinary RO equipment, the LCOW of Ultrasonic-freeze-RO system is reduced by 19.62%, after adding ultrasonic vibration, the LCOW is reduced by 23.70%, to 0.486$/m^3. However, compared with the freeze desalination method with or without ultrasonic vibration, the economic growth is not significant. This is due to the high cost of large ultrasonic vibration equipment. The SWC of Ultrasonic-Freeze-RO system is reduced by 11.10% compared with Freeze-RO. These results reveal that the ultrasonic vibration-based method can effectively reduce both the desalination cost and energy consumption of the freeze desalination method.

Table 16 Performance of desalination systems.

Parameter	Ultrasonic-Freeze-RO	Freeze-RO	RO[38]
SWC/ kWh/m^3	2.922	3.287	/
LCOW/ $/m^3	0.486	0.512	0.637

5 Conclusion

An innovative ultrasonic freezing desalination method has been evaluated through lab-scale experiments. A specially designed ultrasonic freezing crystallizer was used to conduct experiments on ultrasonic-based seawater freezing desalination. These experiments were then compared to traditional methods without the influence of ultrasound. The main conclusions drawn are as follows:

1. Freezing time and temperature exert significant influences on the desalination rate and icing rate of seawater. The salinity of seawater exhibits a more pronounced impact on the experimental outcomes in the absence of ultrasonic vibration compared to its presence.

2. Ultrasonic vibration results in the formation of smaller ice crystals and helps

reduce salt encapsulation, significantly improving the desalination rate of seawater during freezing. Within the salinity range of 15-35 ppt, the desalination rate increased by 18.18% to 67.86%, with a more pronounced effect observed at higher salinity levels. The average desalination rate increased by approximately 32.62%.

3. Ultrasonic vibration promotes the formation of ice crystals and enhances the separation of water molecules and salt ions, leading to an average icing rate increase of 8.03% to 8.20%.

4. Enhancement effect of ultrasound on freezing desalination diminishes with increasing stages of desalination in continuous freezing desalination processes, especially after significant reduction in salinity.

5. The ultrasonic vibration-based method can effectively reduce both the desalination cost and energy consumption of the freeze desalination method. Its specific work consumption is 2.922 kWh/m^3, an 11.10% reduction compared to the Freeze-RO method. The levelized cost of water for the Ultrasonic-Freeze-RO method is \$0.486/m^3, 5.08% lower than the Freeze-RO method and 31.07% lower than the traditional RO method.

Reference

1. Mishra, R.K., *Fresh water availability and its global challenge.* British Journal of Multidisciplinary Advanced Studies, 2023. **4**(3): p. 1-78.
2. Kariman, H., A. Shafieian, and M. Khiadani, *Small scale desalination technologies: A comprehensive review.* Desalination, 2023. **567**: p. 116985.
3. UNDESA, *The Millennium Development Goals Report 2015*. 2016. p. 55.
4. Hu, Z. and Y. Chen, *Advancements in sustainable desalination with ocean thermal energy: A review.* Desalination, 2024. **586**: p. 117770.
5. Shannon, M.A., et al., *Science and technology for water purification in the coming decades.* Nature, 2008. **452**(7185): p. 301-310.
6. Almasoudi, S.M. and J. Bassam, *Desalination technologies and their environmental impacts: A review.* Sustainable Chemistry One World, 2024: p. 100002.
7. Kaviani, R., et al., *Experimental and theoretical study of a novel freeze desalination system with an intermediate cooling liquid.* Desalination, 2024. **576**: p. 117381.
8. Moharramzadeh, S., et al., *Parametric study of the progressive freeze concentration for desalination.* Desalination, 2021. **510**: p. 115077.
9. Harby, K., et al., *Reverse osmosis hybridization with other desalination techniques:*

An overview and opportunities. Desalination, 2024. **581**: p. 117600.

10. Năstase, G., et al., *Advantages of isochoric freezing for food preservation: A preliminary analysis.* International Communications in Heat Mass Transfer 2016. **78**: p. 95-100.

11. Ni, N., et al., *Theoretical research on ship desulfurization wastewater freezing desalination system driven by waste heat.* Desalination, 2023. **549**.

12. Williams, P.M., et al., *Technology for freeze concentration in the desalination industry.* Desalination, 2015. **356**: p. 314-327.

13. Görgüç, A., et al., *Cryoprotective role of vacuum infused inulin on the quality of artichoke: Interactive effects of freezing, thawing and storage period.* Cryobiology, 2024. **116**: p. 104914.

14. Yoda, T., H. Miyaki, and T. Saito, *Freeze concentrated apple juice maintains its flavor.* Scientific Reports, 2021. **11**(1): p. 12679.

15. Petzold, G., et al., *Vacuum-assisted block freeze concentration applied to wine.* Innovative Food Science & Emerging Technologies, 2016. **36**: p. 330-335.

16. Lin, W., M. Huang, and A. Gu, *A seawater freeze desalination prototype system utilizing LNG cold energy.* International Journal of Hydrogen Energy, 2017. **42**(29): p. 18691-18698.

17. Farahat, M.A., et al., *Experimental investigation of freezing desalination using silicon oil for ice production.* Desalination, 2023. **560**: p. 116664.

18. Ong, C.W. and C.-L. Chen, *Technical and economic evaluation of seawater freezing desalination using liquefied natural gas.* Energy, 2019. **181**: p. 429-439.

19. Eghtesad, A., et al., *Numerical investigation and optimization of indirect freeze desalination.* Desalination, 2020. **481**: p. 114378.

20. Jayakody, H., R. Al-Dadah, and S. Mahmoud, *Numerical investigation of indirect freeze desalination using an ice maker machine.* Energy Conversion and Management, 2018. **168**: p. 407-420.

21. Yuan, H., et al., *Theoretical and experimental investigation of an absorption refrigeration and pre-desalination system for marine engine exhaust gas heat recovery.* Applied Thermal Engineering, 2019. **150**: p. 224-236.

22. Lan, W., et al., *Comprehensive thermodynamic and economic analysis of an LNG cold energy recovery system using organic Rankine cycle and freezing-centrifugal desalination for power and water cogeneration.* Journal of Cleaner Production, 2024. **461**: p. 142677.

23. Chang, J., et al., *Freeze desalination of seawater using LNG cold energy.* Water research, 2016. **102**: p. 282-293.

24. Mandri, Y., et al., *Parametric study of the sweating step in the seawater desalination process by indirect freezing.* Desalination, 2011. **269**(1): p. 142-147.

25. Shishiny, A.M., et al., *An investigation of a proposed freezing desalination system integrating sweating effect and a Centrifugal-Based brine rejection technique.* Separation and Purification Technology, 2025. **353**: p. 128390.

26. Hou, Y., et al., *Cellulose nanocrystals facilitate needle-like ice crystal growth and modulate molecular targeted ice crystal nucleation.* Nano Letters, 2021. **21**(11): p. 4868-4877.

27. Mochizuki, K., Y. Qiu, and V. Molinero, *Promotion of homogeneous ice nucleation*

by soluble molecules. Journal of the American Chemical Society, 2017. **139**(47): p. 17003-17006.

28. Wang, Z., et al., *Research on energy saving of ultrasonic wave in the process of making sea-slurry ice.* Energy Conversion and Management, 2021. **247**: p. 114541.

29. Gao, P., et al., *Study on droplet freezing characteristic by ultrasonic.* Heat Mass Transfer, 2017. **53**: p. 1725-1734.

30. Gai, S., et al., *Ice nucleation of water droplet containing solid particles under weak ultrasonic vibration.* Ultrasonics Sonochemistry, 2021. **70**: p. 105301.

31. Tian, Y., et al., *Development of a single/dual-frequency orthogonal ultrasound-assisted rapid freezing technique and its effects on quality attributes of frozen potatoes.* Journal of Food Engineering, 2020. **286**: p. 110112.

32. Daghooghi-Mobarakeh, H., V. Subramanian, and P.E. Phelan, *Experimental study of water freezing process improvement using ultrasound.* Applied Thermal Engineering, 2022. **202**: p. 117827.

33. Zhang, Y., et al., *Promotional effects of ultrasound and oscillation on sea ice desalination.* Separation and Purification Technology, 2024. **347**: p. 127622.

34. Cong, J., et al., *Droplet freezing phase transition and heat transfer under the ultrasonic effect.* International Communications in Heat and Mass Transfer, 2021. **123**: p. 105136.

35. Chen, Z., et al., *Alternating current poling conditions determination by orthogonal experimental design.* Ceramics International, 2024.

36. Nafey, A.S. and M.A. Sharaf, *Combined solar organic Rankine cycle with reverse osmosis desalination process: Energy, exergy, and cost evaluations.* Renewable Energy, 2010. **35**(11): p. 2571-2580.

37. Yi, S., et al., *Pre-expansion ejector absorption power cycle for ocean thermal energy conversion.* Energy Conversion and Management, 2022. **269**: p. 116151.

38. Caldera, U., D. Bogdanov, and C. Breyer, *Local cost of seawater RO desalination based on solar PV and wind energy: A global estimate.* Desalination, 2016. **385**: p. 207-216.

Appendix. Orthogonal experimental design table

Group	**Factors**		
	A	**B**	**C**
1	L1	L1	L1
2	L1	L2	L2
3	L1	L3	L3
4	L1	L4	L4
5	L1	L5	L5
6	L2	L1	L2
7	L2	L2	L3
8	L2	L3	L4
9	L2	L4	L5
10	L2	L5	L1
11	L3	L1	L3
12	L3	L2	L4
13	L3	L3	L5
14	L3	L4	L1
15	L3	L5	L2
16	L4	L1	L4
17	L4	L2	L5
18	L4	L3	L1
19	L4	L4	L2
20	L4	L5	L3
21	L5	L1	L5
22	L5	L2	L1
23	L5	L3	L2
24	L5	L4	L3
25	L5	L5	L4

the salinity of the inlet seawater in the cold storage tank, the temperature of the propylene glycerol-water solution, and the freezing time